

The Low Frequency Instrument for the Payload for Ultrahigh Energy Observations (PUEO)

Yuchieh Ku^{a,*} for the PUEO collaboration

^a*The Pennsylvania State University,
State College, PA, USA*

E-mail: yuchieh@psu.edu

The Payload for Ultrahigh Energy Observations (PUEO) long-duration balloon experiment is designed to observe ultra-high energy (UHE) neutrinos with energies above EeV. PUEO consists of a Main Instrument (MI) on a fixed gondola and a Low Frequency (LF) instrument that will be deployed under the main gondola when the balloon reaches the stratosphere. The LF instrument includes 8 sinuous antennas that operate in the 50-500 MHz range, complementing the 96 dual-polarized horn antennas constituting the MI, designed to receive signals in the 300-1200 MHz range. The LF instrument is sensitive to impulsive, geomagnetic radio signals emitted from air showers, which can be induced by cosmic rays or earth-skimming tau neutrinos. This contribution will report the design and construction status of the LF instrument, encompassing the antennas, the gondola, and the trigger. The expected sensitivity of the MI and the LF instruments to Earth-skimming tau neutrinos and the cosmic rays will also be presented.

*10th International Workshop on Acoustic and Radio EeV Neutrino Detection Activities,
11th-14th June 2024
Chicago, USA*

*Speaker

1. Introduction

The Payload for Ultrahigh Energy Observation (PUEO) [1] is a balloon experiment designed to detect Ultra-High Energy (UHE) neutrinos through radio signals. Currently under construction and scheduled to fly in 2025, PUEO will operate at an altitude of approximately 40 km, circling the Antarctic continent. By scanning 1.5 million square kilometers of ice, PUEO will become the most sensitive detector for UHE neutrinos with energies exceeding 100 EeV.

PUEO features two primary detection channels: the Askaryan channel and the Extensive Air Shower (EAS) channel. The Askaryan channel is designed to observe the Askaryan radiation emitted from particle showers that occur when a neutrino interacts with ice, with a signal predominantly in the vertical polarization. The EAS channel, on the other hand, detects radio waves emitted from air showers, which are mainly horizontally polarized due to the nearly vertical magnetic field at the South Pole. The EAS can be induced by cosmic rays (CRs) or earth-skimming tau neutrinos. More details about PUEO's EAS and Askaryan channels are discussed in [2, 3].

PUEO comprises a Main Instrument (MI) and a Low Frequency (LF) instrument. The MI is equipped with 96 dual-polarized horn antennas operating in the 300-1200 MHz range and is optimized for the Askaryan channel. The LF instrument, which will be deployed beneath the main payload when the balloon reaches the troposphere, consists of eight dual-polarized sinuous antennas that receive signals in the 50-500 MHz range. This LF instrument is optimized for the EAS channel. Figure 1(a) illustrates the deployment of these instruments.

2. LF antenna

Each of the eight LF antennas is a sinuous antenna. This type of antenna was proposed for measuring the polarization of the cosmic microwave background [4]. Its planar properties also made it a suitable candidate for conceptual studies in the Exa-Volt Antenna experiment [5], both conducted at microwave frequencies. For the LF instrument, the design has been modified

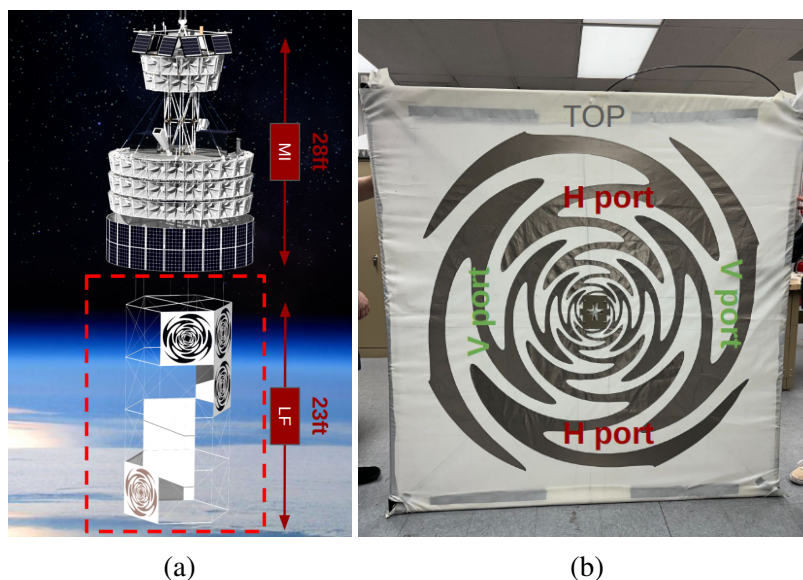


Figure 1: (a) PUEO's main instrument and the LF instrument. (b) Sinuous antenna for the LF instrument. Each antenna is composed of a vertical polarization and a horizontal polarization channels.

[6] and scaled up to 65 inches in diameter for LF's frequency band. The antennas are constructed from nickel-silver conductive fabric sewn onto polyester fabric, chosen to allow compact stowage

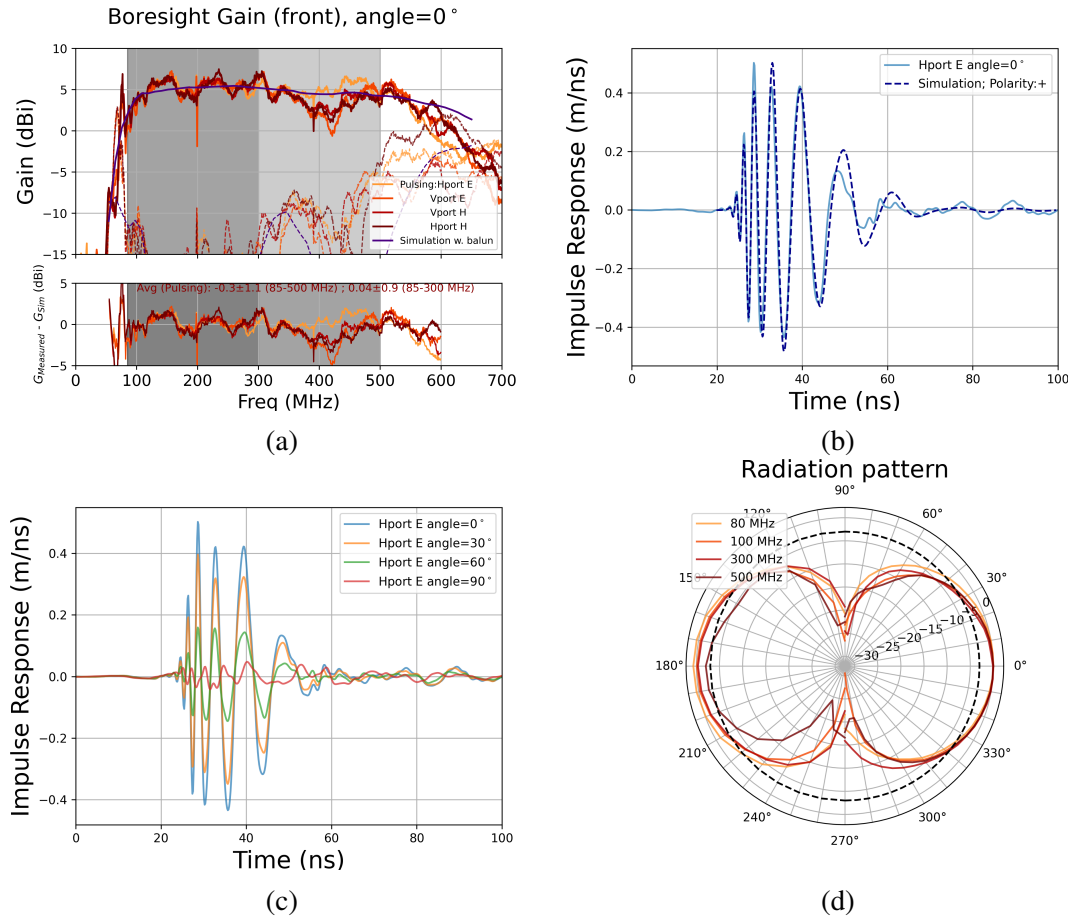


Figure 2: (a) Antenna gain measurement at the boresight axis, for Vpol, Hpol and E and H plane. Dashed curves are contribution from cross polarization. (b) Time domain impulse response of the antenna. (c) Time domain impulse response measured at 0°, 30°, 60° and 90° from the boresight axis. (d) Radiation pattern. The antenna front lobe is centered at 0° and the backlobe at 180°.

in the payload dock before deployment. The antennas are linearly polarized, enabling simultaneous measurement of both horizontal and vertical polarizations. The self-similar arms make the antenna broadband, providing a gain of >3 dBi across a frequency range of 80-500 MHz. The antenna's impedance is theoretically calculated to be 267 ohms [7], and it is impedance-matched through a 4:1 transformer balun. The antenna's properties have been thoroughly characterized through gain, radiation pattern and impulse response measurements, as illustrated in Fig 2. Additionally, the antenna features both front and back lobes with identical performance in both directions.

3. LF array and gondola

The LF array consists of eight sinuous antennas arranged into four layers within a hexagonal gondola, creating horizontal and vertical baselines of 3.1 meters and 5.4 meters, respectively, for interferometry. The hexagonal geometry was chosen over polygons with more sides to maximize the side length and accommodate the size of the antennas. This layout is optimized to achieve

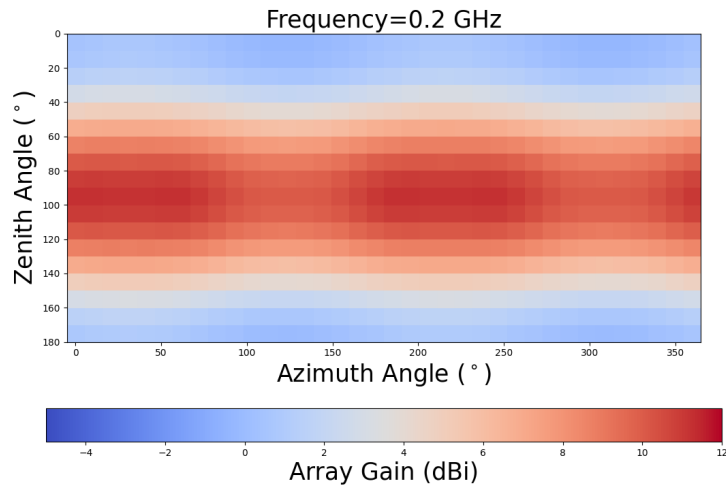


Figure 3: LF instrument array level gain at 200 MHz.



Figure 4: LF instrument deployment mechanism. From left to right is from the storage phase to the deployed phase.

peak gain towards the horizon while providing as uniform gain coverage in the azimuthal direction as possible. The array level gain is shown in Fig 3. Additionally, the design ensures that each antenna is positioned to minimize interference by avoiding overlap in their beam directions. The LF gondola is constructed from carbon fiber tube rings, with layers connected by Dyneema ropes. Upon reaching the stratosphere, the LF will be deployed by releasing ropes constraining the folded array and relying on gravity. Deployment tests, illustrated in the Fig 4, have demonstrated the system's robustness through over forty successful drop tests.

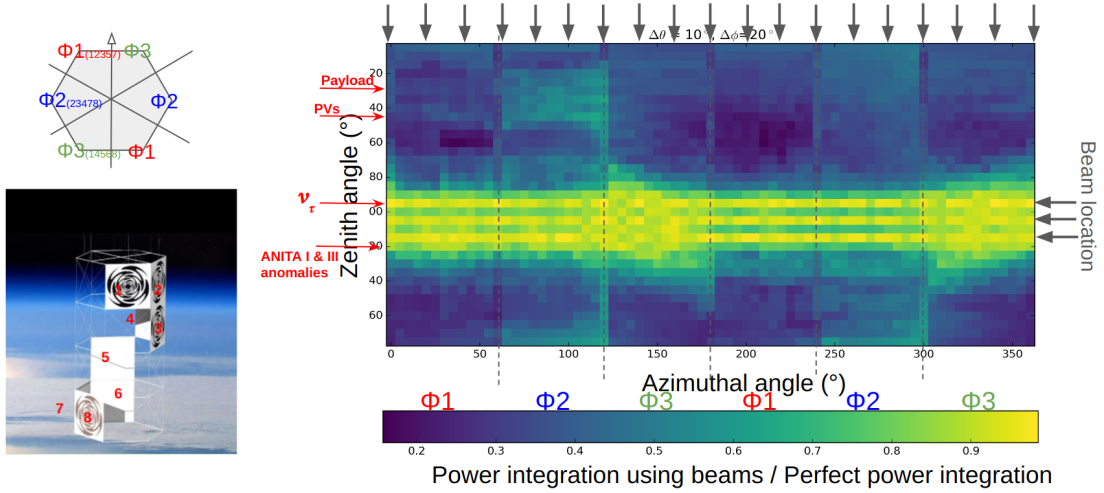


Figure 5: Left: The three azimuthal sectors. The antennas designated to the sector are shown in the parenthesis. Right: The beam map for interferometry. The color map represents the beam efficiency using the 54 beams.

4. LF Trigger Simulation

The LF instrument utilizes an interferometric trigger system, where five of the eight antennas are grouped into an azimuthal sector. Interferometry is achieved by assigning time delays to individual channels based on assumed signal directions, referred to as beams. Within each beam, the delayed waveforms from each channel in the azimuthal sector are summed together. By scanning through the beams, the system performs a coherent sum in the beam that is closest to the actual signal direction. Within each azimuthal sector, any antenna can observe signals within 60° of its boresight axis. Because of this, we form three azimuthal sectors in which five different antennas with overlapping fields-of-view contribute to a given beam. The geometry and the participating antennas in each azimuthal sector are shown in Fig 5. Since the boresight axes of antennas within a sector are not necessarily aligned, it is crucial that the antennas' phase responses remain consistent for signals arriving from different directions. This consistency has been verified through impulse response measurements, as illustrated in Fig 2(c).

In the LF trigger, the number of beams is limited to 54 by the computational resources available in the Radio-Frequency System-on Chip (RFSoc) [1, 8] used in the data acquisition boards. Therefore, these beams are strategically placed in directions where significant scientific observations are expected. For example, the system provides good coverage towards Earth-skimming tau neutrinos, which have peak flux near the horizon, and steep anomalies at elevations around -30° , as identified by ANITA [9, 10]. Conversely, directions toward the payload and solar panels are intentionally left uncovered, indicating low trigger efficiency in these areas, which helps minimize noise interference from the payload. The beam map and the beam efficiency using the beams are shown in Fig 5.

The trigger efficiency is evaluated in the simulation. The targeted event rate for the LF is 1-10 Hz, compared to the 100 Hz for the MI. Based on the event rate, trigger threshold is studied using simulated noise events. The noise model is built with consideration of galactic noise, thermal radiation from the ice, and the RF chain system noise. The trigger efficiency curve from simulations

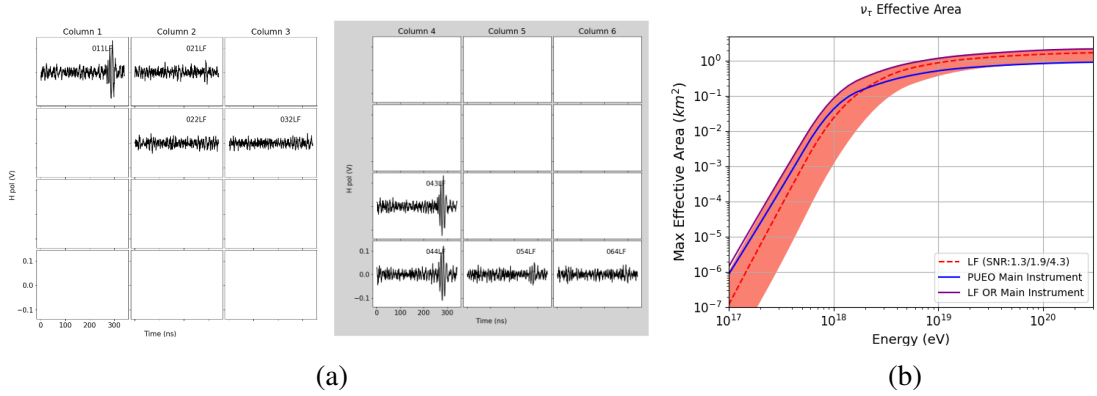


Figure 6: (a) A simulated earth-skimming tau neutrino event and the LF’s detector response. (Hpol channels) The six columns and four rows represent the six sides of the hexagonal array and four vertical layers, respectively. (b) Peak effective area over elevation angle for the ν_τ point source.

indicates that the LF triggers at a single antenna SNR of 1.9, where the SNR is the average of antennas in an azimuthal sector and it is defined by the waveforms that convolves signals to antenna response and the RF chain response. The LF trigger is designed to cooperate with the MI trigger through a mutual ‘or’ configuration, meaning they operate independently but will both save data whenever either instrument triggers.

5. Science Performance in Simulation

The performance of the LF instrument in the EAS channel has been simulated using a combination of three simulation packages: (1) Pueosim [11], (2) CRSim, and (3) TAPIOCA [12]. Pueosim includes a detailed detector model of both the MI and the LF instrument, while CRSim and TAPIOCA serve as event generators that simulate and propagate radio signals initiated by UHECRs and Earth-skimming tau neutrinos, respectively. Although trigger simulations indicate that the LF instrument triggers at a single antenna SNR of 1.9, this has not yet been lab-tested or implemented into the RFSoc. To account for this, three trigger thresholds (SNR = 1.3, 1.9, and 4.3) were simulated, representing pessimistic, realistic, and optimistic scenarios. Figure 6(a) illustrates the simulated response of the LF’s eight horizontal polarization channels to a 100 EeV earth-skimming tau neutrino, where the tau lepton decays, producing an approximately 1 EeV shower.

The tau channel is particularly sensitive to point sources. The peak effective area over elevation angles to a ν_τ point source is shown in Fig 6(b). Compared to the MI, the LF provides a comparable effective area, performing especially well at energies above 10 EeV due to its broader view angle coverage, in contrast to the high-frequency component, which peaks only at the Cherenkov cone. Figure 7 illustrates PUEO’s aperture to reflected CR events and the expected energy spectra during PUEO’s 30-day flight. The reflected CRs are those events where the radio signals reflect off the ice surface before arriving at PUEO. PUEO is anticipated to observe nearly a thousand CR events, with one-third of these triggering both instruments and yielding high SNR in each. The remaining events will trigger either instrument, with both recording the data. The LF’s coverage at lower frequencies will aid in categorizing these CR events, which are a significant background for neutrino searches.

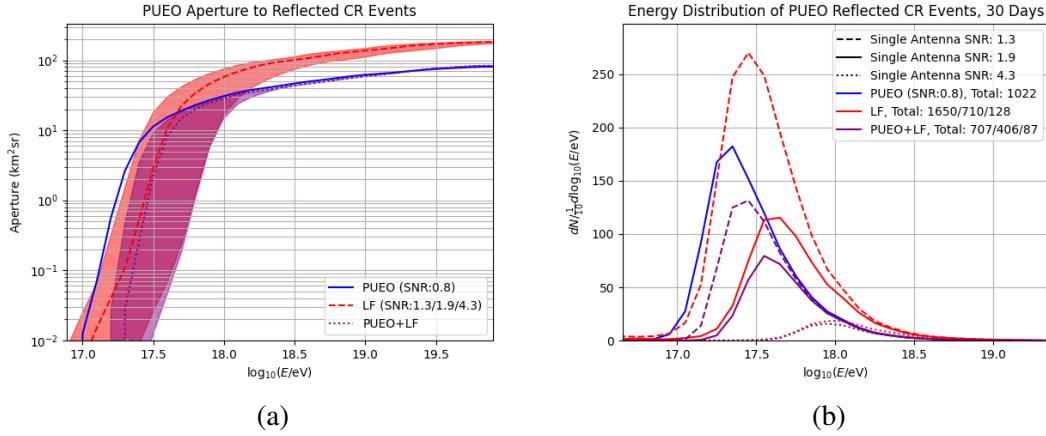


Figure 7: (a) PUEO’s aperture to the reflected CR events. (b) Energy distribution of the reflected CR events. Events detected by both instruments are shown in purple curves.

6. Conclusion

The LF instrument is a critical component of PUEO, providing supplemental low-frequency data to enhance signals detected by the MI. Additionally, the LF instrument increases PUEO’s sensitivity to the EAS channel, making it a valuable standalone detector. The LF antennas and gondola have been successfully built and tested, with the deployment mechanism demonstrating robust performance. Future work includes implementing the LF trigger into the RFSoc and conducting further lab tests. The construction of the LF instrument is progressing in line with PUEO’s scheduled flight in 2025.

References

- [1] Q. Abarr et al. The payload for ultrahigh energy observations (pueo): a white paper. *Journal of Instrumentation*, 16(08):P08035, Aug 2021.
- [2] Kaeli Autumn Hughes et al. Identifying and Characterizing Air Shower Events with the Payload for Ultrahigh Energy Observations (PUEO). *PoS, ICRC2023*:1027, 2023.
- [3] Cosmin Deaconu et al. Searching for Askaryan Emission from Neutrinos with the Payload for Ultrahigh Energy Observations (PUEO). *PoS, ICRC2023*:1031, 2023.
- [4] Yutaro Sekimoto et al. Concept design of low frequency telescope for cmb b-mode polarization satellite litebird. In *Millimeter, Submillimeter, and Far-Infrared Detectors and Instrumentation for Astronomy X*. SPIE, December 2020.
- [5] P.W. Gorham, F.E. Baginski, P. Allison, K.M. Liewer, C. Miki, B. Hill, and G.S. Varner. The exavolt antenna: A large-aperture, balloon-embedded antenna for ultra-high energy particle detection. *Astroparticle Physics*, 35(5):242–256, December 2011.
- [6] Dylan A. Crocker and Waymond R. Scott. On the design of sinuous antennas for uwb radar applications. *IEEE Antennas and Wireless Propagation Letters*, 18(7):1347–1351, 2019.

- [7] Jennifer M. Edwards, Roger O'Brient, Adrian T. Lee, and Gabriel M. Rebeiz. Dual-polarized sinuous antennas on extended hemispherical silicon lenses. *IEEE Transactions on Antennas and Propagation*, 60(9):4082–4091, 2012.
- [8] Keith McBride et al. Design of the PUEO Payload. *PoS*, ARENA2024, 2024.
- [9] P. W. Gorham et al. Characteristics of Four Upward-pointing Cosmic-ray-like Events Observed with ANITA. *Phys. Rev. Lett.*, 117(7):071101, 2016.
- [10] P. W. Gorham et al. Observation of an unusual upward-going cosmic-ray-like event in the third flight of anita. *Phys. Rev. Lett.*, 121:161102, Oct 2018.
- [11] William Luszczak et al. Updated Simulation of Airborne Neutrino Detectors for the PUEO Experiment. *PoS*, ICRC2023:1154, 2023.
- [12] R. Prechelt, S. Wissel, et al. Analysis of a tau neutrino origin for the near-horizon air shower events observed by the fourth flight of the antarctic impulsive transient antenna. *Physical Review D*, 105(4), February 2022.

Full Authors List: PUEO Collaboration

Q. Abarr¹, P. Allison², J. Alvarez-Muñiz³, J. Ammerman Yebra³, T. Anderson⁴, A. Basharina-Freshville⁵, J. J. Beatty², D. Z. Besson⁶, R. Bose⁷, D. Braun⁷, P. Chen⁸, Y. Chen⁸, J. M. Clem¹, T. Coakley², A. Connolly², L. Cremonesi⁹, A. Cummings⁴, C. Deaconu¹⁰, J. Flaherty², P. W. Gorham¹¹, C. Hornhuber⁶, J. Hoffman⁷, K. Hughes², A. Hynous¹², M. Jackson², A. Jung¹¹, Y. Ku⁴, C.-Y. Kuo⁸, G. Leone¹⁰, C. Lin¹, P. Linton², T. C. Liu¹³, W. Luszczak², S. Mackey¹⁰, Z. Martin¹⁰, K. McBride², C. Miki¹¹, M. Mishra¹¹, J. Nam⁸, R. J. Nichol⁵, A. Novikov¹, A. Nozdrina⁶, E. Oberla¹⁰, S. Prohira⁶, R. Prechelt¹¹, H. Pumphrey⁵, B. F. Rauch⁷, R. Scrandis¹⁰, D. Seckel¹, M. F. H. Seikh⁶, J. Shiao^{8,14}, G. Simburger⁷, G. S. Varner¹¹, A. G. Viereggs¹⁰, S.-H. Wang⁸, C. Welling¹⁰, S. A. Wissel^{4,15}, C. Xie⁵, R. Young⁶, E. Zas³, A. Zeolla⁴

¹Dept. of Physics, Univ. of Delaware, Newark, DE 19716.

²Dept. of Physics, Center for Cosmology and AstroParticle Physics, Ohio State Univ., Columbus, OH 43210.

³Instituto Galego de Física de Altas Enerxías (IGFAE), Universidade de Santiago de Compostela, 15782 Santiago de Compostela, Spain

⁴Pennsylvania State Physics Dept., Inst. for Gravitation and the Cosmos, University Park, PA 16802.

⁵Dept. of Physics and Astronomy, University College London, London, United Kingdom.

⁶Dept. of Physics and Astronomy, Univ. of Kansas, Lawrence, KS 66045.

⁷Dept. of Physics, McDonnell Center for the Space Sciences, Washington Univ. in St. Louis, MO 63130.

⁸Dept. of Physics, Grad. Inst. of Astrophys., Leung Center for Cosmology and Particle Astrophysics, National Taiwan University, Taipei, Taiwan.

⁹School. of Physics and Astronomy, Queen Mary University of London, London, United Kingdom.

¹⁰Dept. of Astronomy & Astrophysics, Dept. of Physics, Enrico Fermi Inst., Kavli Inst. for Cosmological Physics, Univ. of Chicago, Chicago, IL 60637.

¹¹Dept. of Physics and Astronomy, Univ. of Hawaii, Manoa, HI 96822.

¹²NASA Wallops Flight Facility, Wallops Island, VA, 23337

¹³Dept. of Physics, National Yang Ming Chiao Tung University, Taipei, Taiwan.

¹⁴National Nano Device Laboratories, Hsinchu 300, Taiwan.

¹⁵Pennsylvania State Astronomy and Astrophysics Dept., University Park, PA 16802.